Synthesis of Biomorphic Charcoal/TiO₂ Composites from Moso Bamboo Templates for Absorbing Microwave

Liangcun Qian,*,[a] Shuyun Yang,[b] Weining Hong,[a] Peirong Chen,[a] and Xiaolin Yao [a]

Biomorphic charcoal/TiO₂ composites (C/TiO₂) from moso bamboo templates were produced for absorbing microwave. Subsequently, the characteristics of the C/TiO₂ were investigated by scanning electron microscopy, thermogravimetric analysis, and vector network analysis. The results showed that the biomorphic microstructure of the moso bamboo charcoal was duplicated in the C/TiO₂. Thus, the density of the C/TiO₂ sintered at 1200 °C was lower and approximately 0.916 ± 0.003 g/cm³. Moreover, the ignition, the maximum combustion, and the burnout temperatures of the C/TiO₂ sintered at 600 °C were ~320 °C, ~530 °C, and ~585 °C, respectively. Additionally, with the rising of the temperature sintering C/TiO₂, the microwave absorbency of the C/TiO₂ was improved over high frequency zones. Furthermore, the average imaginary-part values of the permittivity of the C/TiO₂ sintered at 600 °C and 1200 °C notably increased by 11.16-fold. In addition, the peak of microwave reflection loss of the samples (2.0 mm thickness) from the C/TiO₂ powder (wt. 20%) sintered at 1200 °C and the paraffin wax (wt. 80%) was observed as -18.0 dB at 17.4 GHz. Therefore, the C/TiO₂ sintered at higher temperatures exhibited lower geometrical density, better thermostability, and favorable microwave absorptive properties.

*Contact information: a: School of Science and b: School of Resources and Environment, Anhui Agricultural University, Hefei, 230036, P. R. China;*Correspondence author: qianliangc@126.com*

INTRODUCTION

With the use of the various communication tools, including high power microwave generators, our daily environment has become filled with microwave interference, microwave pollution, and radar (Petrov and Gagulin 2001; Chen *et al.* 2007; Zou *et al.* 2010). Thus, microwave absorbing materials have been widely researched, *e.g.* the dielectric/magnetic materials, metal materials, conjugated polymers (CPs), CNTs, graphene, and their various combinations (composites/blends/hybrids) with the outstanding absorbing properties (Dang *et al.* 2014; Saini 2015; Verma *et al.* 2015a). However, due to their higher densities, the dielectric/magnetic and metal materials have been excluded from usage in light-weight microwave absorbers (Kim *et al.* 2004; Wang *et al.* 2012). Although the CPs with lower densities can be used in light-weight microwave absorbers, difficulties have been encountered in applying to higher temperature circumstance owing to their uncertain thermostability. CNTs and graphene with the characteristics of low density, high electrical conductivity, and high thermostability can be regarded as suitable candidates, but they have disadvantages with lower dielectric constants (Verma *et al.* 2015b). According of the principle of electromagnetic interference shielding, electric field energy can be stored in a combination of the dielectric materials and is proportional to the relative

dielectric constant of the materials under the stable electric field (Abbas *et al*. 2006; Saini and Arora 2013; Dang *et al.* 2014). Moreover, under an alternating electromagnetic field, the dielectric is polarized through the rotation of electric moment and displacement of the electron cloud. Furthermore, electric field energy is converted into heat energy by fast moving charge dissipation (Phang *et al.* 2008; Dang *et al.* 2014). Therefore, the various composites of CNTs and graphene structure with dielectric materials have become a focus for the development of absorbing microwave materials (Chung 2012; Saini 2015; Verma *et al*. 2015a).

Bamboo charcoal sintered at high temperature exhibits characteristics of low density and a structure similar to that of CNTs and graphene (Jiang *et al*. 2004), which makes it an attractive material in microwave absorbers. Also, its dielectric constant is lower. However, titanium dioxide (TiO_2) has a larger static dielectric constant (Xia *et al*. 2013). Thus, TiO_2 was anticipated to increase the dielectric constant of the composite. Additionally, the use of natural wood and charcoal templates for inorganic materials is an effective strategy to obtain controllable materials with biomorphic microstructure (Qian *et al*. 2015; Li *et al*. 2016; Qian *et al*. 2016). Further, owing to the porous microstructure of bamboo, it is accessible to gaseous or aqueous infiltration and suitable for producing porous biomorphic composites (Li *et al*. 2014; Chen *et al*. 2015). Therefore, the charcoal/TiO_2 composite from moso bamboo templates can be prepared and become an alternative candidate for microwave absorbing materials.

In this work, the infiltration behavior of butyl titanate sol was investigated with moso bamboo templates. Vacuum/positive pressure technology was used to initiate sol-gel infiltration into the pores of moso bamboo. Subsequently, the C/TiO_2 was sintered from the templates of the moso bamboo in a N_2 atmosphere. The biomorphic structures, crystalline phase, sol impregnation effect, thermostability, and microwave absorbing properties of the C/TiO_2 were characterized by scanning electron microscopy (SEM), thermogravimetric analysis (TGA), X-ray diffraction (XRD), and vector network analysis (VNA), respectively. Additionally, the density, thermostability, and absorbing properties of the C/TiO_2 were compared with other microwave absorbent materials.

EXPERIMENTAL

Materials and Reagents

Chemical-grade butyl titanate ($Ti(OC_4H_9)_4$) and analytical-grade acetic acid (CH_3COOH), and anhydrous ethanol (CH_3CH_2OH) were purchased from the Sinopharm Chemical Reagent Co., Ltd., Shanghai, China. All reagents were used without further purification. The purity of nitrogen (N_2) was 99.999%.

Specimens of moso bamboo were harvested from the Forest Farm of She County, Anhui Province, China. Native moso bamboo stems were from plants more than or equal to 5 yrs old, and the specimens were cut into chips with a radial thickness of 6.02 ± 0.01 mm, a tangential width of 15.32 ± 0.02 mm, and an average axial length of 10.03 ± 0.02 mm (excluding the exterior part and interior part of moso bamboo along the radial direction). All chips were heated in a microwave oven at 1200 W for 10 min with water, and then the water was replaced. The above heating process was repeated 10 times. Finally, all samples were dried at 90 °C for 24 h.

Composites Preparation

$Ti(OC_4H_9)_4$, CH_3COOH, and CH_3CH_2OH (volume ratio of 68:12:50) were stirred for 2 h at room temperature to obtain the TiO_2 sol. The dried samples were immersed in TiO_2 sol for 7 days and subsequently subjected to infiltration in an adjustable air pressure dipping can at a vacuum pressure of 1.0 kPa for 30 min and a positive air pressure of 2.0 MPa for 30 min. Finally, all samples were removed from the sol. The sol of moso bamboo templates absorbed water from air for 12 h, resulting in the formation of $Ti(OC_4H_9)_4$ gelatin, CH_3COOH, and CH_3CH_2OH. All samples were dried at 130 °C for 2 h so that the TiO_2 gel moved into cell cavities. To produce the C/TiO_2, all samples were pyrolyzed in N_2 (GLS-1700X).

A furnace containing a vacuum tube (GLS-1700X, Kexing Materials Co., Ltd., China) was used for sintering the samples. The temperature program was set as follows: 20 °C to 400 °C at a heating rate of 1 °C/min; 400 °C to the maximum temperature of 600 °C, 700 °C, 800 °C, 950 °C, and 1200 °C in N_2, respectively, at a heating rate of 2 °C/min; the maximum temperature was maintained for 1 h; and the maximum temperature to room temperature cooling rate of -2 °C/min. After the sintering process, the samples were pyrolyzed at various temperatures to produce the C/TiO_2.

Manufacture Microwave Absorbers

The scattering parameters and properties of microwave absorbers are relevant to the absorbing microwave component, percent of absorbing units, and the thickness of the absorbers (Petrov and Gagulin 2001; Saini 2015). Referring to the manufacturing methods of microwave absorbers in the correlative literatures (Kim *et al.* 2005; Wang *et al*. 2015), after the above C/TiO_2 were ground into a powder, the fine powder was sifted through a sieve with an average pore diameter of 100 μm. The C/TiO_2 powder and paraffin wax (mass ratio of 2:8) were homogeneously mixed and stirred at 60 °C for 2 h, and the specimens were manufactured into microwave absorbers of toroidal shape with a thickness of 2.0 mm and an inner diameter of 3.0 mm.

Characterization

The anatomic structures of the biomorphic charcoal and the C/TiO_2 from the moso bamboo templates were observed under a scanning electron microscope (S-4800, Hitachi, Tokyo, Japan). The phase structure of TiO_2 after sintering was identified using an X-ray diffractometer (XD-3, Persee, Beijing, China), operating with Cu Kα radiation ($λ = 1.540563$ Å), a scan rate of 1°/min, an accelerating voltage of 36 KV, an applied current of 20 mA, and a diffraction angle ($2θ$) ranging from 10° to 70°.

A thermogravimetric analyzer (TG-209, NETZSCH, Selb, Germany) was used to measure the thermostability of the C/TiO_2, and it was operated with a purged air flow rate of 20 mL/min. The C/TiO_2 powder (10.0 mg) was loaded into an alumina crucible on the thermogravimetric analyzer and heated at 10 °C/min from 40 °C to 700 °C. The corresponding mass remnants (TiO_2) and thermostability of the C/TiO_2 were analyzed using thermogravimetric-differential thermogravimetric (TG-DTG) profiles. The slope of the TG profile equaled the speed of mass loss (MS). The DTG profiles also expressed the rate of MS. According to Eq. 1, the value of T was defined as the temperature when the differential of the DTG profile equaled zero, *i.e.*, the inflection point for temperature in the DTG profiles. Therefore, T_1, T_2, and T_3 represented the ignition temperature at the first

inflection point of the DTG profile, the burnout temperature at the last inflection point of the DTG profile, and the temperature of the maximum combustion rate in the bottom inflection point of the DTG profile, respectively,

$$\frac{d^3 M\%}{dt^3} = 0 \tag{1}$$

where M is the mass of the powder and t is the temperature of the powder in the crucible.

The scattering parameters (ε', μ', ε'', and μ'') of the toroidal-shaped absorbers were measured using a vector network analyzer (E5071C, Agilent, CA, USA) in the frequency range of 2 GHz to 18 GHz. The relative permeability (μ_r) and permittivity (ε_r) values were calculated using Eq.2 and 3 (Petrov and Gagulin 2001; Wang *et al.* 2012),

$$\varepsilon_r = \varepsilon' - j\varepsilon'' \tag{2}$$

$$\mu_r = \mu' - j\mu'' \tag{3}$$

where ε' and μ' are the real-part values of the relative permittivity (ε_r) and permeability (μ_r); ε'' and μ'' are the imaginary-part values of the ε_r and μ_r, respectively. According to the above electromagnetic parameters and the transmission line theory (Wang *et al.* 2012), the input impedance (Z_{in}) of the absorber interface can be calculated as follows,

$$Z_{in} = Z_0 (\frac{\mu_r}{\varepsilon_r})^{1/2} \tanh\left\{ j\left(\frac{2\pi f d}{c} \right)(\mu_r \varepsilon_r)^{1/2} \right\} \tag{4}$$

where f is the frequency, d is the thickness of the absorber, c is the velocity of the light, and Z_0 is the impedance of air. The reflection loss (RL, dB) of the microwave at the absorber surface is given by Eq. 5 (Saini 2015; Verma *et al.* 2015a):

$$RL = 20 \log\left| \frac{Z_{in} - Z_0}{Z_{in} + Z_0} \right| \tag{5}$$

Density Measurements

The mass of the samples (M) was measured using a balance with the precision of 0.001 g. The sample volume (V) was measured using vernier calipers with the precision of 0.01 mm. Densities (ρ) were calculated using Eq. 6:

$$\rho = \frac{M}{V} \tag{6}$$

RESULTS AND DISCUSSION

Microstructure Analysis

Figures 1a and 1b show the SEM images of moso bamboo charcoal sintered at 800 °C in N_2. The different sizes and distributions of the pores were visualized from the formation. The first pipe pores originated from the big vessels in Fig. 1a, with pore diameters of approximately 150 μm in the transverse section. The second and third pipe pores originated from the smaller pipes and parenchymas, with pore sizes of 5 μm to 10 μm parallel to the fibers and 10 μm to 30 μm in the transverse section (the top-right of Fig. 1a). The fourth pipe pores originated from the fibers with pore diameters of 3 μm to 8 μm

in the axial section (the left of Fig. 1b). The pits in the cell walls (approximately 1 μm in diameter) were visualized in the axial section (the right of Fig. 1b). Because the pits were smaller and less numerous, sol embolisms were destroyed in these pipes during the vacuum/positive pressure process of sol infiltration. Thus, sol was impregnated completely and homogenously on the moso bamboo templates using this method. Figure 1c shows the SEM images of the C/TiO_2 from the moso bamboo templates sintered at 600 °C in N_2. For the C/TiO_2 composites, the cell cavity of the big vessels, small pipes, and parenchymas were incompletely filled by TiO_2 crystal grains. Additionally, all of the pipe pores maintained the microstructure of moso bamboo charcoal.
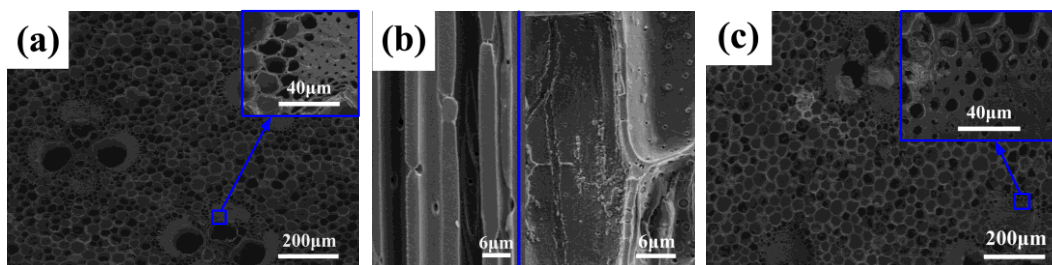

Fig. 1. SEM of moso bamboo charcoal and charcoal/TiO_2 composites: (a) transverse section (100X magnification); small pipes and parenchymas of the transverse section (500X magnification on the top-right figure); (b) fibers of the axial section on the right (500X magnification); and parenchymas of the axial section on the left (1500X magnification); and (c) the charcoal/TiO_2 composites of transverse section (100X magnification) and small pipe (500X magnification on the top-right figure)

Density Measurements

Table 1 shows the geometrical densities of the moso bamboo charcoals and the C/TiO_2 sintered at various temperatures. The maximum density of the moso bamboo charcoal and C/TiO_2 were 0.614 ± 0.003 and 0.916 ± 0.003 g/cm^3, respectively. Moreover, the densities increased with the sintering temperature. However, the density of rutile TiO_2 is 4.26g/cm^3 (Xia *et al.* 2013), and the density of ordinary metal and magnetic materials is greater than 1.00 g/cm^3 (Kim *et al.* 2004). Because of the hollow and porous microstructure of charcoal, the moso bamboo charcoal and the C/TiO_2 were lower in density.

Table 1. Density of Moso Bamboo Charcoal and Charcoal/TiO_2 Composites Sintered at Various Temperatures

Carbonization Temperature (°C)	Mean Geometrical Density ± Standard Deviation (g/cm^3)	
	Moso bamboo charcoal	C/TiO$_2$
600	0.557 ± 0.002	0.815 ± 0.003
700	0.581 ± 0.002	0.849 ± 0.003
800	0.597 ± 0.002	0.874 ± 0.003
950	0.603 ± 0.003	0.897 ± 0.004
1200	0.614 ± 0.003	0.916 ± 0.003

TiO₂-Phase Formation

The TiO₂-phase formations of the C/TiO₂ were evaluated by XRD analysis during the heat treatment by pyrolyzing charcoal under a N₂ atmosphere between 700 °C and 1200 °C (Fig. 2). The diffraction peaks at 25.2°, 37.8°, 48.1°, and 55.2° were assigned to the diffractions of the (101), (004), (200), and (211) planes of anatase TiO₂, respectively (JCPDS number 21-1272) (Yang *et al*. 2009). The diffraction peaks at 27.5°, 36.0°, 41.5°, and 54.0° were assigned to the diffractions of the (110), (101), (200), and (211) planes of rutile TiO₂, respectively (JCPDS number 21-1276) (Xia *et al*. 2013). The phase transformation shift from anatase to rutile was similar to that of poplar templates. As the temperature increased, the diffraction peaks of TiO₂ became steeper. Thus, the crystalline structure of TiO₂ was more perfect (Qian *et al*. 2015). After the TiO₂ phase transformation shifted from anatase to rutile, the static dielectric constant of TiO₂ increased from 48 to 180 (Phang *et al*. 2008). Consequently, the rutile phase of the C/TiO₂, sintered at a higher temperature, was anticipated to absorb more microwaves. Further, their dielectric constants and *RL* with the microwave frequency were measured and discovered.
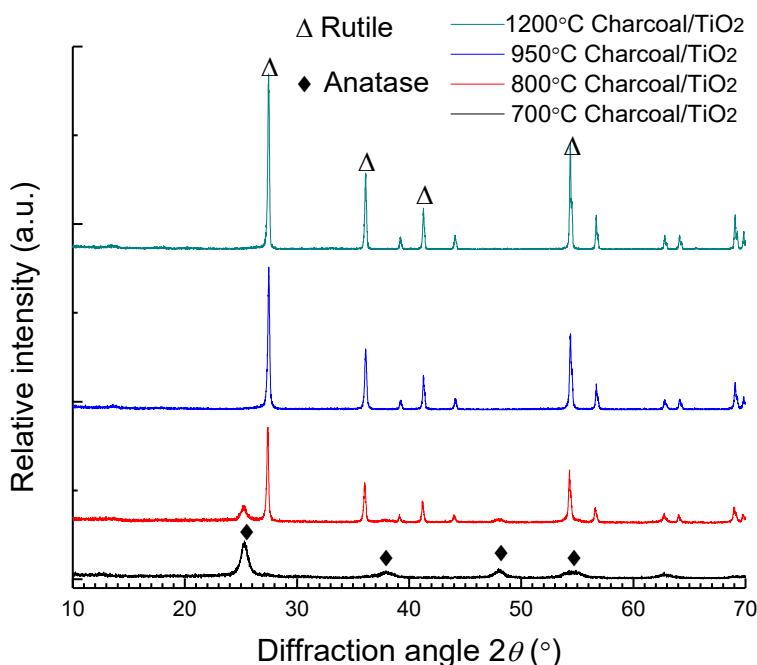

Fig. 2. X-ray diffraction patterns of moso bamboo charcoal/TiO₂ composites

Microwave Absorbing Properties

Generally, there are dielectric and magnetic absorbing units in microwave absorbing materials (Abbas *et al*. 2006; Chen *et al*. 2007). The microwave absorbent properties of materials are expressed by the complex permittivity and complex magnetic permeability (Wang *et al.* 2012). The real-part values (ε' and μ') of complex permittivity and magnetic permeability are related to the storage capacity of electrical and magnetic energy in the materials, respectively; however, the imaginary-part values (ε'' and μ'') are related to the dissipation (or loss) capacity of electrical and magnetic energy of the materials, respectively (Abbas *et al*. 2006; Zou *et al*. 2010; Saini 2015; Zhang *et al*. 2015). In addition, the loss tangent of the dielectric/magnetic can be expressed as $\tan\delta_E = \varepsilon''/\varepsilon'$ and

$\tan\delta_M = \mu''/\mu'$ respectively. Hence, a microwave absorbing material is expected to constantly increase its imaginary part and decrease its real part in the electromagnetic parameters.

The actual power level (0.25 mW) of the incident microwave radiation was used for the measurements. Figures 3a and 3b show the curves of the relative complex dielectric constants, ε' and ε'', of the microwave absorbents manufactured by using moso bamboo C/TiO_2, sintered at 600 °C (600 C/TiO_2), 950 °C (950 C/TiO_2), and 1200 °C (1200 C/TiO_2), respectively.
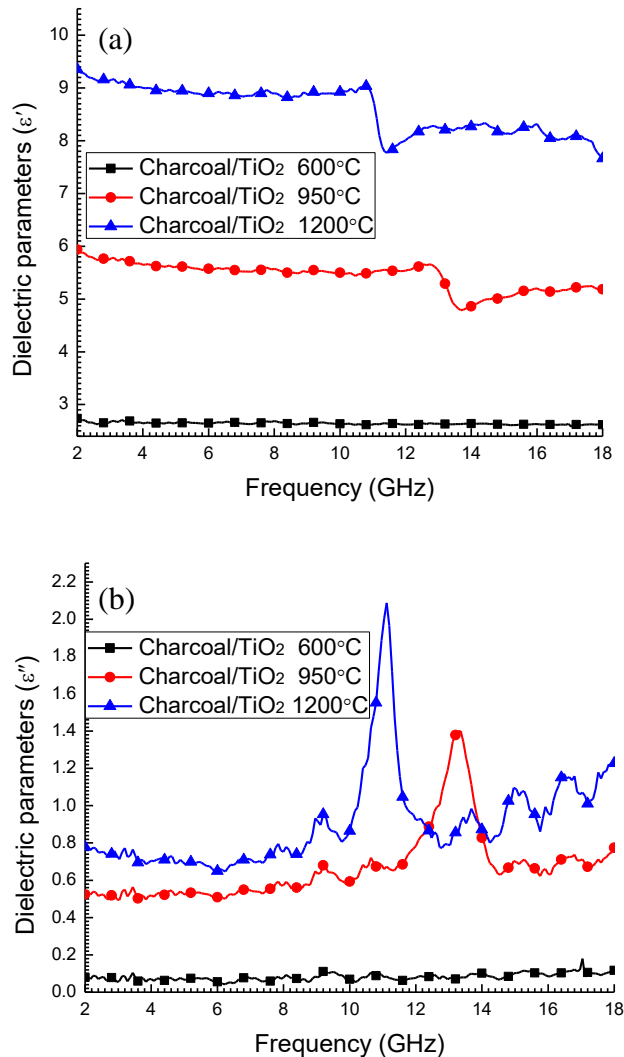

Fig. 3. The relative complex permittivity: (a) real parts (ε´) and (b) imaginary parts (ε")

Both ε' and ε'' of 600 C/TiO_2 maintained constant values with increasing microwave frequency; their average values were 2.642 and 0.081, respectively. The average values of ε' and ε'' of 950 C/TiO_2 were 5.438 and 0.666; likewise the average values of 1200 C/TiO_2 were 8.600 and 0.904, respectively. As the sintering temperature increased, ε' and ε'' notably increased. When the sintering temperature increased from 600 °C to 1200 °C, the average real-part values increased from 2.642 to 8.600 (3.26-fold amplification). However, the average imaginary-part values increased from 0.081 to 0.904

(11.16-fold amplification). Therefore, as the sintering temperature increased, both the storage and the dissipation (or loss) capacity of electrical energy in the materials were improved. Nevertheless, the dissipation (or loss) capacity was enhanced more rapidly than the storage capacity of electrical energy, which was in favor of the improvement on $\tan\delta_E$ and decreasing the *RL* of the materials (Saini 2015). The values of $\varepsilon´$ in 950 C/TiO$_2$ decreased rapidly from 12.72 GHz to 13.68 GHz, and the $\varepsilon´$ of 1200 C/TiO$_2$ decreased rapidly from 10.80 GHz to 11.44 GHz. Thereafter, the values of $\varepsilon´$ were maintained. In contrast, the ε'' of 950 C/TiO$_2$ and 1200 C/TiO$_2$ increased rapidly to the peak value of 13.36 GHz and 10.96 GHz, respectively. The results showed that a higher sintering temperature improved both the storage and dissipation capability of the electric field energy of the C/TiO$_2$. Previous reports showed that a higher calcination temperature improves the graphitization degree and the conductivity of bamboo charcoal, which may be an important reason for the loss of electric field energy in the C/TiO$_2$ (Jiang *et al*. 2004).

Figures 4a and 4b show the $\mu´$ and μ'' values of 600C/TiO$_2$, 950C/TiO$_2$, and 1200C/TiO$_2$ from 2 GHz to 18 GHz.
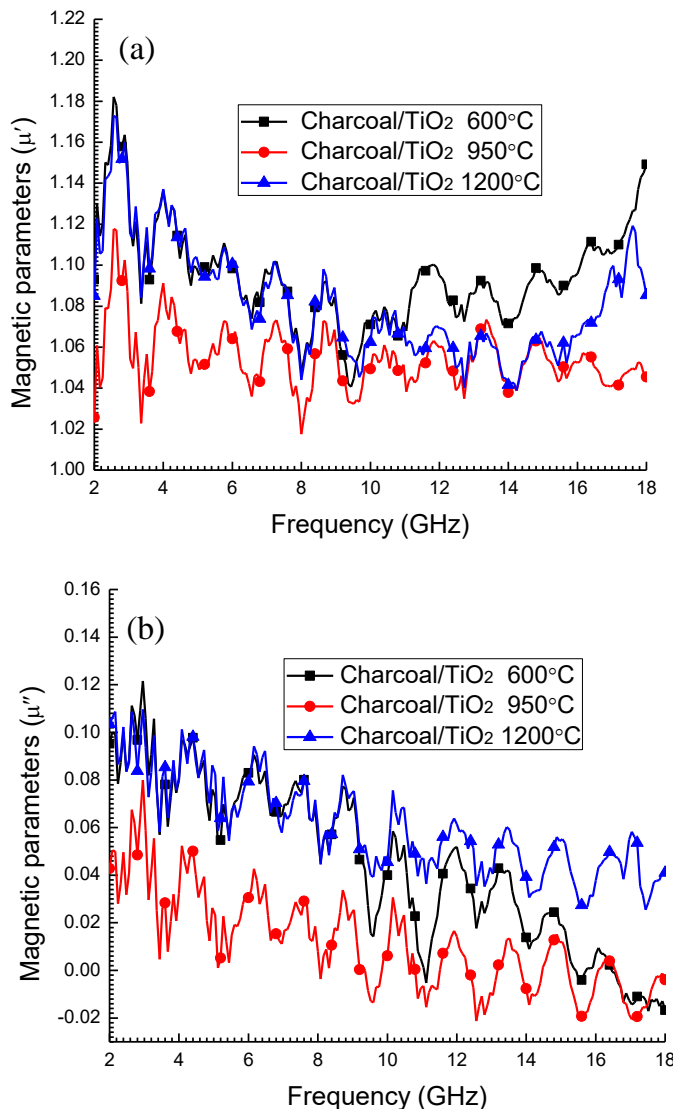

Fig. 4. The relative complex permeability: (a) real parts ($\mu´$) and (b) imaginary parts (μ'')

The average real-part values of μ' for 600 C/TiO$_2$, 950 C/TiO$_2$, and 1200 C/TiO$_2$ were 1.095, 1.055, and 1.076, respectively. Likewise, the average imaginary-part values of μ'' for 600 C/TiO$_2$, 950 C/TiO$_2$, and 1200 C/TiO$_2$ were 0.045, 0.011, and 0.062, respectively. With the change in calcination temperature, the average values of μ' were approximately equal; the average μ'' decreased initially and then increased slightly. Consequently, the sintering temperature almost had less effect on the storage capacity of the magnetic energy of C/TiO$_2$. However, the values of μ'' fluctuated and decreased slightly from 2 GHz to 18 GHz. Thus, the sintering temperature decreased slightly the magnetic loss capacity. As the measurement frequency increased, the storage capabilities of the magnetic energy in the C/TiO$_2$ slightly increased above 9.5 GHz, but the dissipation capabilities of magnetic energy slightly declined. The results showed that the calcination temperature minimally affected the storage and dissipation capabilities of the magnetic energy in the C/TiO$_2$. The above results and phenomena were caused owing to the very weak magnetic properties of the C/TiO$_2$ (Xia *et al.* 2013). Therefore, the absorbing microwave of the C/TiO$_2$ mainly was focused on the dielectric properties.

An important factor in absorbency is an outstanding *RL* value from the surface of absorbent (Liu *et al*. 2007; Wang *et al*. 2012; Li *et al*. 2015). Therefore, *RL* values were calculated at a given frequency, percent of the C/TiO$_2$, and absorbent thickness using Eq. 5. Figure 5 shows the *RL* values of 600 C/TiO$_2$, 950 C/TiO$_2$, and 1200 C/TiO$_2$ from 2 GHz to 18 GHz. The *RL* values of 600 C/TiO$_2$ were equal to 0 dB; however, the *RL* values of 950 C/TiO$_2$ were started with 9 GHz and terminated at 17 GHz. Furthermore, the best *RL* value was -9.64 dB at 15.6 GHz. 1200 C/TiO$_2$ (from 9 GHz to 18 GHz) notably exhibited the stronger performance of absorbing microwave. Moreover, the *RL* peak value for 1200 C/TiO$_2$ was -18.0 dB at 16.8 GHz. The absorbency performance of 1200C/TiO$_2$ was equal to that of hybrid MoS$_2$ and reduced graphene oxide, as previously reported (Wang *et al*. 2015). With increasing calcination temperature, the *RL* peak of the C/TiO$_2$ shifted to the high frequency region. Additionally, the *RL* amplitude of C/TiO$_2$ was enlarged. This change should be attributed to the development of the graphitization degree in the bamboo charcoal and the crystallization degree of the TiO$_2$.
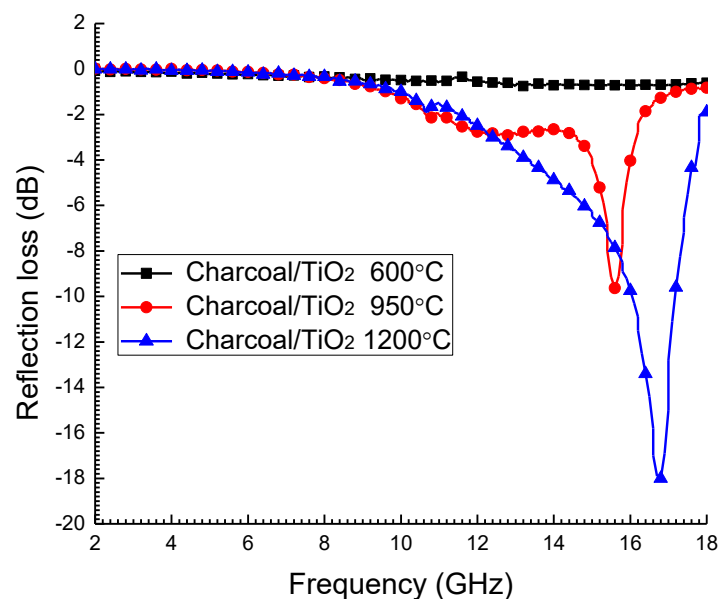

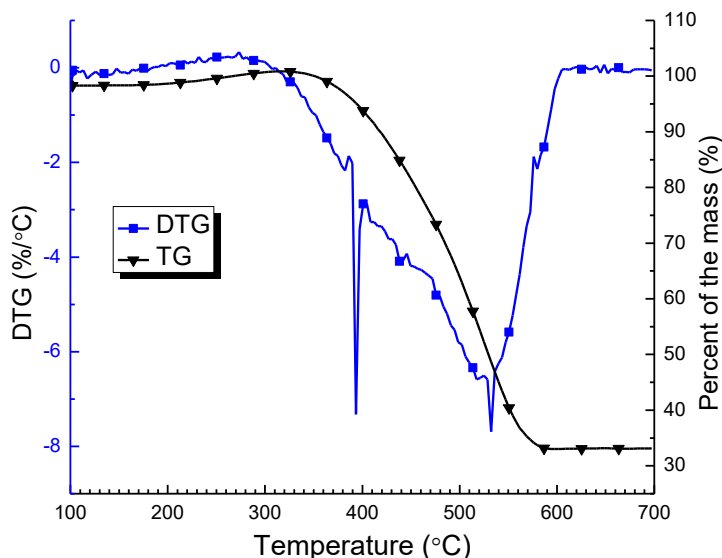**Fig. 5.** The reflection loss of microwaves related to the frequency values

Fig. 6. The TG-DTG curves of the bamboo charcoal/TiO_2 composites sintered at 600 °C in N_2

Thermogravimetric and Differential Thermogravimetric Analyses

The TG-DTG curves expressed the thermostability of the heated C/TiO_2 (Mahr *et al*. 2012). Figure 6 shows the TG-DTG curves of 600 C/TiO_2 below 700 °C in an air atmosphere. The 600 C/TiO_2 composite (below 340 °C) was stable in an air atmosphere. The corresponding remnant (TiO_2) was estimated at approximately 31.46%. The ignition temperature (T_1), burnout temperature (T_2), and temperature of the maximum combustion rate (T_3) were determined by using Eq. 2. The DTG curves revealed that the T_1, T_2, and T_3 of 600 C/TiO_2 were approximately 320 °C, 530 °C, and 585 °C, respectively (Fig. 6). The DTG curve appeared to shift from 380 °C to 400 °C, corresponding to a faster combustion rate at 390 °C. The above phenomenon was attributed to the tight packing of TiO_2 around the charcoal on the surface of C/TiO_2, hindering oxygenolysis. Moreover, the ignition temperature of the 600 C/TiO_2 composite was higher than that of the poplar C/TiO_2 sintered at 400 °C (Qian *et al*. 2016). Thus, the TG-DTG results showed that the C/TiO_2 were better thermostability in an air circumstance.

CONCLUSIONS

The hollow biomorphic C/TiO_2 from templates of moso bamboo charcoal exhibited the characteristics of lower density, better thermostability, and outstanding properties of absorbing microwave. Their maximum density was only 0.916 ± 0.003 g/cm^3 in the 1200 C/TiO_2, and the ignition temperature of 600 C/TiO_2 had reached for 320 °C. When the thickness of the absorbent (wt. 20% of the C/TiO_2 power) was only of 2.0 mm, the absorbing amplitude of 1200 C/TiO_2 was -18 dB at 16.8 GHz. As the calcination temperature increased, the storage and dissipation capability of the electric field energy were improved; favorable *RL* values of the C/TiO_2 shifted to the high frequency region and the *RL* amplitude was increased.

ACKNOWLEDGEMENTS

REFERENCES CITED

Abbas, S. M., Chandra, M., Verma, A., Chatterjee, R., and Goel, T. C. (2006). "Complex permittivity and microwave absorption properties of a composite dielectric absorber," *Composites Part A Applied Science & Manufacturing* 37(11), 2148-2154. DOI: 10.1016/j.compositesa.2005.11.006

Chen, N., Mu, G., Pan, X., Gan, K., and Gu, M. (2007). "Microwave absorption properties of $SrFe_{12}O_{19}/ZnFe_2O_4$ composite powders," *Materials Science & Engineering B* 139(2-3), 256-260. DOI: 10.1016/j.mseb.2007.02.002

Chen, Q., Endo, T., and Wang, Q. (2015). "Characterization of bamboo after ionic liquid-H_2O pretreatment for the pyrolysis process," *BioResources* 10(2), 2797-2808. DOI: 10.15376/biores.10.2.2797-2808

Chung, D. D. L. (2012). "Carbon materials for structural self-sensing, electromagnetic shielding and thermal interfacing," *Carbon* 50(9), 3342–3353. DOI: 10.1016/j.cabon.2012.01.031

Dang, Z., Yuan, J., Yao, S., and Liao, R. (2014). "Flexible nanodielectric materials with high permittivity for power energy storage," *Advanced Materials* 45(3), 6334-6365. DOI: 10.1002/adma.201301752

Jiang, Z. H., Zhang, D. S., Fei, B. H., Yue, Y. D., and Chen, X. H. (2004). "Effects of carbonization temperature on the microstructure and electrical conductivity of bamboo charcoal," *Xinxing Tan Cailiao/New Carbon Materials* 19(4), 249-253. DOI: 1007-8827(2004)04-0249-05

Kim, S. S., Kim, S. T., Ahn, J. M., and Kim, K. H. (2004). "Magnetic and microwave absorbing properties of Co–Fe thin films plated on hollow ceramic microspheres of low density," *Journal of Magnetism & Magnetic Materials* 271(1), 39-45. DOI: 10.1016/j.jmmm.2003.09.012

Kim, S. S., Kim, S. T., Yoon, Y. C., and Lee, K. S. (2005). "Magnetic, dielectric, and microwave absorbing properties of iron particles dispersed in rubber matrix in gigahertz frequencies," *Journal of Applied Physics* 97(10), 10F905:1-4. DOI: 10.1063/1.1852371

Li, D., Ma, X., Liu, X., and Yu, L. (2014). "Preparation and characterization of nano-TiO_2-loaded bamboo-based activated carbon fibers by H_2O activation," *BioResources* 9(1), 602-612. DOI: 1015376/biores.9.1. 602-612

Li, G., Wang, L., Li, W., and Xu, Y. (2015). "Fe-, Co-, and Ni-loaded porous activated carbon balls as lightweight microwave absorbents," *Chemphyschem* 16(16), 3458-3467. DOI: 10.1002/cphc.201500608

Li, R., Shu, Z., Qian, L., Zhou, L., Liu, Y., and Liu, S. (2016). "Magnetic biomorphic $BaFe_{12-x}Cr_xO_{19}$ ceramics with multilayer wall structure made from spruce templates," *BioResources* 11(2), 3937-3946. DOI: 1015376/biores.11.2.3937-3946

Liu, Z., Bai, G., Huang, Y., Ma, Y., Du, F., Li, F., Guo, T., and Chen, Y. (2007). "Reflection and absorption contributions to the electromagnetic interference shielding of single-walled carbon nanotube/polyurethane composites," *Carbon* 45(4), 821-827. DOI: 10.1016/j.carbon.2006.11.020

Mahr, M. S., Hübert, T., Sabel, M., Schartel, B., Bahr, H., and Militz, H. (2012). "Fire retardancy of sol–gel derived titania wood-inorganic composites," *Journal of Materials Science* 47(11), 6849-6861. DOI: 10.1007/s10853-012-6628-3

Petrov, V. M., and Gagulin, V. V. (2001). "Microwave absorbing materials," *Inorganic Materials* 37(2), 93-98. DOI: 0020-1685/01/3702-0093

Phang, S. W., Tadokoro, M., Watanabe, J., and Kuramoto, N. (2008). "Microwave absorption behaviors of polyaniline nanocomposites containing TiO_2 nanoparticles," *Current Applied Physics* 8(3-4), 391-394. DOI: 10.1016/j.cap.2007.10.022

Qian, L., Li, R., Zhou, L., Liu, Y., Yu, M., Xiong, F., Liu, S., and Hao, X. (2015). "Preparation of biomorphic TiO_2 ceramics from Rattan templates," *BioResources* 10(3), 4391-4402. DOI: 1015376/biores.10.3.4391-4402

Qian, L., Chen, P., Li, R., Mei, L., Liu, Y., Wu, G., and Liu, S. (2016). "Biomorphic charcoal/TiO_2 composites from Poplar templates," *BioResources* 11(2), 3432-3441. DOI: 1015376/biores. 11.2.3432-3441

Saini, P. (2015). "Intrinsically conducting polymer-based blends and composites for electromagnetic interference shielding: Theoretical and experimental aspects," in: *Fundamentals of Conjugated Polymer Blends, Copolymers and Composites: Synthesis, Properties and Applications*, P. Saini (ed.), John Wiley & Sons, Inc., Hoboken, NJ, USA, Edition: 1, Chapter: 9. DOI: 10.1002/9781119137160.ch9

Saini, P. and Arora, M. (2013). "Formation mechanism, electronic properties & microwave shielding by nano-structured polyanilines prepared by template free route using surfactant dopants," *Journal of Materials Chemistry A* 1(31), 8926-8934. DOI: 10.1039/c3ta11086a

Su, B. L. (2012). "Hierarchically structured porous materials for energy conversion and storage," *Advanced Functional Materials* 22(22), 4634-4667. DOI: 10.1002/adfm.201200591

Verma, P., Saini, P., and Choudhary, V. (2015a). "Designing of carbon nanotube/polymer composites using melt recirculation approach: Effect of aspect ratio on mechanical, electrical and EMI shielding response," *Materials & Design*, 88, 269-277. DOI: 10.1016/j.matdes.2015.08.156

Verma, P., Saini, P., Malik, R. S., and Choudhary, V. (2015b). "Excellent electromagnetic interference shielding and mechanical properties of high loading carbon-nanotubes/polymer composites designed using melt recirculation equipped twin-screw extruder," *Carbon*, 89, 308-317. DOI: 10.1016/j.carbon.2015.03.063

Wang, C., Han, X., Xu, P., Zhang, X., Du, Y., Hu, S., Wang, J., and Wang, X. (2012). "Response to "Comment on 'The electromagnetic property of chemically reduced graphene oxide and its application as microwave absorbing material'" [Appl. Phys. Lett. 100, 046101 (2012)]," *Applied Physics Letters* 100(4), 046102-046101. DOI: 10.1063/1.3678193

bioresources.com

Wang, Y. , Chen, D., Yin, X., Xu, P., Wu, F., and He, M. (2015). "Hybrid of MoS_2 and reduced graphene oxide: A lightweight and broadband electromagnetic wave absorber," *ACS Applied Materials & Interfaces* 7(47), 26226-26234. DOI: 10.1021/acsami.5b08410

Xia, T., Zhang, C., Oyler, N. A., and Chen, X. (2013). "Hydrogenated TiO_2 nanocrystals: A novel microwave absorbing material," *Advanced Materials* 25(47), 6905-6910. DOI: 10.1002/adma.201303088

Yang, D., Liu, H., Zheng, Z., Yuan, Y., Zhao, J., Waclawik, ER., Ke, X., and Zhu, H. (2009). "An efficient photocatalyst structure: TiO_2 (B) nanofibers with a shell of anatase nanocrystals," *Journal of the American Chemical Society* 131(49), 17885-17893. DOI: 10.1021/ja906774k

Zhang, X., Ji, G., Liu, W., Quan, B., Liang, X., Shang, C., Cheng, Y., and Du, Y. (2015). "Thermal conversion of an Fe_3O_4 metal-organic framework: A new method for an efficient Fe-Co/nanoporous carbon microwave absorbing material," *Nanoscale* 7(30), 12932-12942. DOI: 10.1039/C5NR03176A

Zou, T., Li, H., Zhao, N., and Shi, C. (2010). "Electromagnetic and microwave absorbing properties of multi-walled carbon nanotubes filled with Ni nanowire," *Journal of Alloys & Compounds* 496(1-2), L22-L24. DOI: 10.1016/j.jallcom.2010.02.103